Round-Trip Oxidative Addition, Ligand Metathesis, and Reductive Elimination in a P^{III}/P^{V} Synthetic Cycle

Soohyun Lim and Alexander T. Radosevich*

Department of Chemistry, Massachusetts Institute of Technology, 77 Massachusetts Avenue, Cambridge, MA 02139, United States

Supporting Information Placeholder

ABSTRACT: A synthetic cycle for aryl C–F substitution comprising oxidative addition, ligand metathesis, and reductive elimination at a C_s-symmetric phosphorus triamide (**1**, P{N[*o*-NMe–C_6H_4]$_2$}) is reported. Reaction of **1** with perfluoroarenes (Ar^F–F) results in C–F oxidative addition yielding fluorophosphoranes **1**•[F][Ar^F]. The *P*-fluoro substituent is exchanged for hydride by treatment with DIBAL-H, generating hydridophosphoranes **1**•[H][Ar^F]. Heating of **1**•[H][Ar^F] regenerates **1** by C–H reductive elimination of Ar^F–H, where experimental and computational studies establish a concerted but highly asynchronous mechanism. The results provide well-characterized examples of the full triad of elementary mechanistic aryl C–X substitution steps at a single main-group site.

Oxidative addition, ligand metathesis (transmetalation), and reductive elimination are the elementary mechanistic steps by which numerous aryl C–X substitution reactions are enabled. Round-trip sequencing of these steps is well-known for the late transition metals, enabled by the kinetically and thermodynamically favorable two-electron redox reactivity of the *d*-block elements.[1] Despite significant recent advances in oxidative addition (OA) and reductive elimination (RE) at main-group element centers,[2,3] the realization of an analogous mechanistic triad with *p*-block elements is beset by poor energetic parity among oxidation states $E^{n/n+2}$ that favors unidirectional OA or RE. For instance, low-valent group 13/14 compounds cleave aryl C–X bonds by OA (Figure 1A, *left*),[4-9] but RE from high-valent compounds of these electropositive elements is rare.[10,11] Complementarily, aryl C–H RE from high-valent Group 16/17 compounds have been described (Figure 1B, *right*),[12-15] but OA to the low-valent state of such electronegative elements is challenging.

The central position of the group 15 elements within the *p*-block results in moderate electronegativities and accessible $E^{III/V}$ redox couples[16-19] useful for aryl functionalization. Recent excellent examples by McNally[20] (for heteroaryl functionalization via a $P^V \rightarrow P^{III}$ RE step) and Cornella[21] (for functionalization of aryl boron compounds via a $Bi^V \rightarrow Bi^{III}$ RE step) are paradigmatic; nonetheless the high-valent arylpnictogen(V) intermediates are accessed via the use of an exogenous oxidant (S^{VI} reagent in the former, 'F^+' reagent in the latter), not aryl C–X OA. Indeed, while both OA[22-24] and RE[12,25] are independently known within the P^{III}/P^{V} couple, no single system exhibits the full suite of elementary steps in the aryl C–X substitution mechanism. Here, we report well-defined stoichiometric reactions atop a single phosphorus platform that trace a closed P^{III}/P^{V} synthetic loop comprising aryl C–F OA and aryl C–H RE interposed with F→H ligand metathesis (Figure 1B).[26] These results establish the redox equipoise of the P^{III}/P^{V} couple as required for OA/RE round-tripping, providing a further basis for forward-going development of group 15 promoted aryl C–X substitution chemistry.

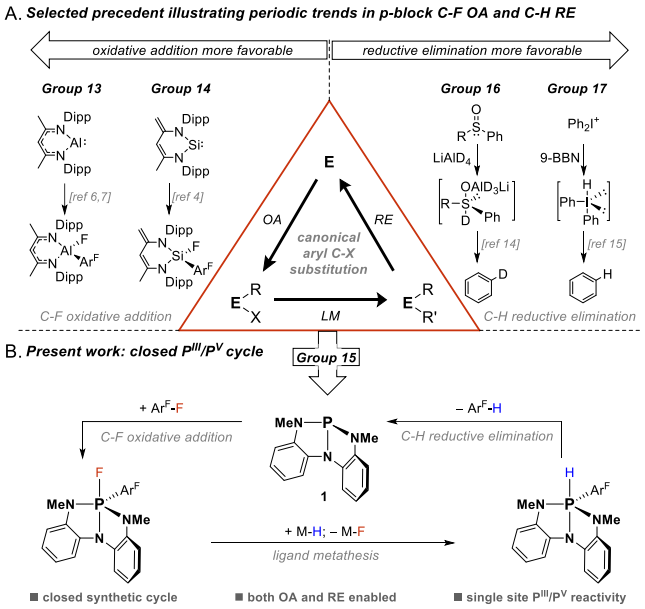

Figure 1. (A) Selected examples of main-group oxidative addition and reductive elimination reactions. (*left*) C–F oxidative addition to Group 13/14 compounds; (*right*) C–H reductive elimination from Group 16/17 compounds. (B) Phosphorus-centered two-electron redox cycle for aryl C–F substitution.

On the basis of prior research showing that C_s-symmetric σ^3-phosphorus triamide **1** undergoes reversible OA/RE of amine N–H substrates,[23] we considered whether this compound would be energetically poised to support the targeted elementary aryl substitution reactions. As depicted in Figure 2, reaction of **1** with the perfluoroarenes—aryl C–X compounds otherwise known as nucleophilic aromatic substitution (S_NAr)

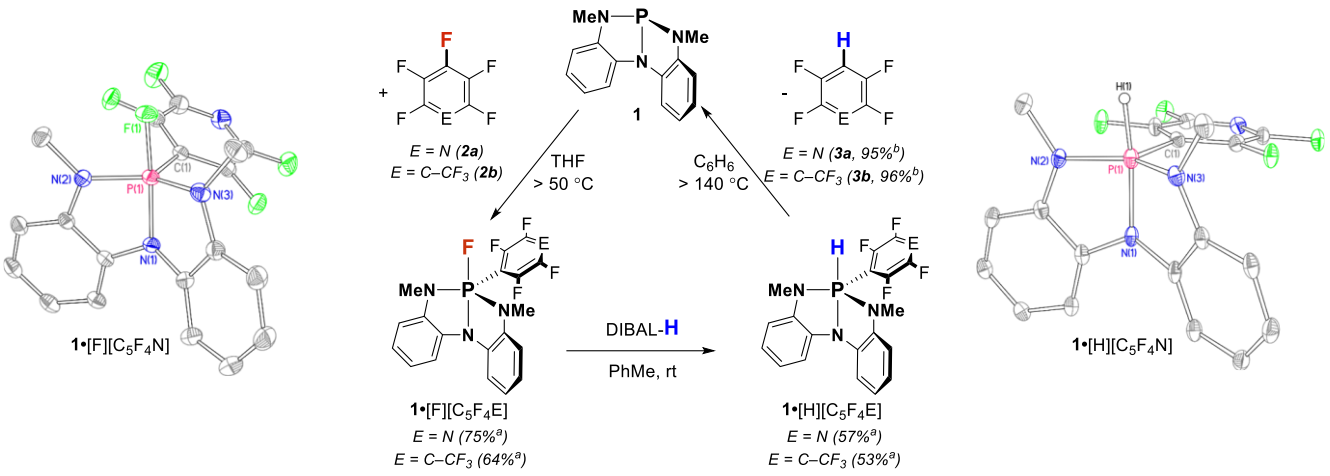

Figure 2. P^{III}/P^{V} synthetic cycle on **1** comprising aryl C–F oxidative addition, F→H ligand metathesis, and C–H reductive elimination. Thermal ellipsoid plots of intermediates **1**•[F][C_5F_4N] (left) and **1**•[H][C_5F_4N] (right) are rendered at the 50% probability level. Hydrogen atoms except H(1) in **1**•[H][C_5F_4N] are omitted for clarity. [a] Isolated yield. [b] Internal standard yield by NMR.

substrates—was selected for investigation.[27] Treatment of **1** with pentafluoropyridine (**2a**, >2 equiv) in tetrahydrofuran above 50 °C leads to the clean consumption of **1** and formation of a new species with spectral features consistent with C–F OA product **1**•[F][C_5F_4N]. The large upfield shift of the ^{31}P NMR resonance for **1**•[F][C_5F_4N] (δ –61.0 ppm) compared to **1** (δ +159.8 ppm) conforms with expectations for an increase in *P*-coordination number, and the further presence of a large coupling constant ($^1J_{P-F}$ = 768.8 Hz) confirms the formation of a P–F bond. ^{19}F NMR spectra show complementary coupling to a fluorine-19 nucleus (δ –34.67 ppm; $^1J_{F-P}$ = 765.7 Hz). Related C–F OA reactivity is observed upon reaction of **1** with other perfluoroarenes (viz. perfluorotoluene **2b** gives **1**•[F][$C_5F_4CF_3$] and perfluorobenzonitrile gives **1**•[F][C_5F_4CN]),[28] although not for simple arylfluorides.[29] σ^3-P Compounds are known to undergo addition to electron-deficient haloarenes by S_NAr, but stable σ^5-P adducts by C–F OA are not formed.[30,31] The unique reactivity of **1** is attributable to its unusual biphilicity;[32] analogous OA was not observed with common phosphorus triamides.[33]

The fluorophosphoranes obtained by C–F OA to **1** are indefinitely stable in solution at ambient temperature; diffraction quality single crystals deposit from concentrated solutions in diethyl ether upon cooling. By X-ray diffraction analysis, the solid-state structure of **1**•[F][C_5F_4N] adopts a pentacoordinate geometry intermediate between trigonal bipyramidal and square pyramidal extrema along the Berry coordinate, biased somewhat toward the former (τ = 0.60[34]). Indeed, as represented in the thermal ellipsoid plot in Figure 2 (left), the *P*-fluoro substituent of **1**•[F][C_5F_4N] is distal, but not rigorously apical, with respect to the diarylamino N_1; the fluoroheteroaryl group similarly deviates from an idealized equatorial position (Table 1). By structural comparison to known fluorophosphorane compounds, the $P_1–F_1$ bond length of **1**•[F][C_5F_4N] (1.6282(6) Å) is short relative to the average apical P–F distance (1.650 Å).[35] For reference, **1**•[F][C_5F_4N] shows a $P–F_{ax}$ distance and IR stretching frequency (687 cm^{-1}) intermediate of the polyfluorophosphoranes $MePF_4$ (1.612 Å, 720 cm^{-1}) and Me_2PF_3 (1.643 Å, 648 cm^{-1}).[36] Given the known correlation of $P–F_{ax}$ bond energy and electronegativity of the ancillary ligands,[37] we infer a high affinity of the phosphorus center for the fluoride substituent in **1**•[F][C_5F_4N][38] (*vide infra*).

Table 1. Tabulated bond distances (Å), angles (°), and δ (ppm) values for selected compounds.[a]

Metric	**1**[b]	**1**•[F][C_5F_4N]	**1**•[H][C_5F_4N]
$d(P_1–N_1)$	1.7610(12)	1.7616(8)	1.778(2)
$d(P_1–N_2)$	1.7014(14)	1.6841(9)	1.698(2)
$d(P_1–N_3)$	1.7190(13)	1.6753(9)	1.695(2)
$d(P_1–F_1/H_1)$	—	1.6282(6)	1.347(19)
$d(P_1–C_1)$	—	1.8456(10)	1.884(2)
$\angle N_1–P_1–F_1/H_1$	—	174.28(4)	172.7(10)
$\angle N_1–P_1–C_1$	—	95.62(4)	94.31(9)
$\angle N_2–P_1–N_3$	115.21(7)	139.66(5)	139.41(10)
δ ^{31}P	159.8	–61.0	–62.7

[a] See SI for full details. [b] Data from Ref. 23.

Consistent with the short P–F distance, fluoride abstraction from **1**•[F][C_5F_4N] was not accessible by treatment with $B(C_6F_5)_3$ (FIA = 107.1 kcal/mol)[39]; however, the addition of the more potent fluoride acceptor $Al(C_6F_5)_3$ (FIA = 130.0 kcal/mol) did result in fluoride transfer and formation of **1**•$[C_5F_4N]^+[AlF(C_6F_5)_3]^-$ as observed by ^{31}P NMR spectroscopy (δ +54.3 ppm). Likewise, **1**•[F][C_5F_4N] is unreactive to common borane reagents (9-BBN, HBcat) but undergoes smooth reaction instead with diisobutylaluminum hydride (DIBAL-H, 1.5 equiv) in toluene at room temperature. In this latter reaction, ^{31}P NMR spectra are consistent with an exchange of fluoride for hydride at the pentacoordinate phosphorus (δ –62.7 ppm), formulated as hydridophosphorane **1**•[H][C_5F_4N] (Figure 2); a doublet resonance with large coupling constant ($^1J_{P-H}$ = 541.7 Hz) collapses to a singlet upon proton decoupling, corroborating the presence of the P–H bond. **1**•[F][$C_5F_4CF_3$] also transforms to **1**•[H][$C_5F_4CF_3$] in the same conditions. The requirement for a strongly fluorophilic metathesis reagent would seem to imply a significant stepwise character to the exchange reaction.

Structural determination of **1**•[H][C_5F_4N] was undertaken by X-ray diffraction on a single-crystalline sample, wherein the phosphorus-bound hydrogen atom (H_1) was located in the dif-

ference Fourier map and refined isotropically. Modest distinctions are noted when comparing **1**•[F][C_5F_4N] and **1**•[H][C_5F_4N]; as depicted in Figure 2 (right), the intermediate trigonal bipyramidal/square pyramidal geometry of **1**•[F][C_5F_4N] is largely retained in **1**•[H][C_5F_4N] (τ = 0.56). With the less electronegative H substituent in place of F, a slight lengthening of the remaining four bonds to P is observed (Table 1). Overall, the geometry of **1**•[H][C_5F_4N] is comparable to the reported structures of the other hydridophosphorane molecules derived from **1**,[23] where the *P*-hydrido substituent occupies a distal position from N_1 (viz. $\angle N_1–P_1–H_1$ = 167-176°).

A solution of **1**•[H][C_5F_4E] (E = N or C–CF_3, 5-100 mM in C_6D_6) sealed in an NMR tube is stable at ambient temperature, but heating above 140 °C results in the consumption of the starting material. Time-stacked ^{31}P NMR spectra (Figure 3a) indicate that **1**•[H][C_5F_4N] (δ –62.5 ppm) is reverted to **1** (δ +160.4 ppm) through an apparent C–H RE from phosphorus(V). Simultaneous monitoring within the ^{19}F NMR channel (Figure 3b) confirms the concomitant formation of RE product 2,3,5,6-tetrafluoropyridine **3a**. Quantitative ^1H NMR analysis of the reaction under these conditions establish that the reaction proceeds cleanly (ca. 95% mass recovery).

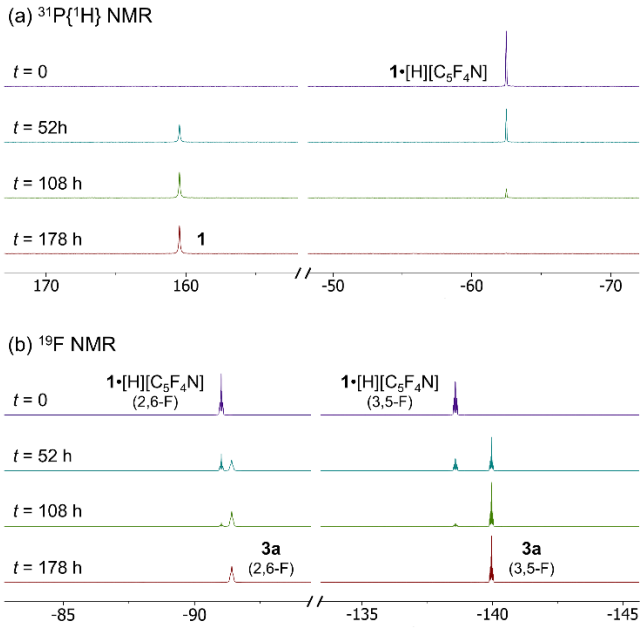

Figure 3. Time-stacked (a) $^{31}P\{^1H\}$ NMR and (b) ^{19}F NMR spectra of **1**•[H][C_5F_4N] in C_6D_6 at *t* = 0, 52, 108, and 178 h at 160 °C. Units are ppm relative to 85% H_3PO_4 (^{31}P) and $CFCl_3$ (^{19}F). See SI for unabridged spectra.

To further characterize the nature of this C–H RE, the reaction kinetics were evaluated at 160 °C by quantitative ^1H NMR spectroscopy using durene as an internal standard. As shown in Figure 4a, the concentration of **1**•[H][C_5F_4N] decays according to first-order kinetics, with a rate constant $k = 6.38\pm0.01 \times 10^{-6}$ s^{-1}. Isotope labelling studies confirm the intramolecular provenance of the C-H coupling partners; heating a solution of **1**•[D][C_5F_4N] exclusively generated D–C_5F_4N. Independentkinetic profiling of the C-H RE for **1**•[H][C_5F_4N] and **1**•[D][C_5F_4N] establish a kinetic isotope effect of k_H/k_D = 1.17±0.11.[40] Furthermore, a crossover experiment by heating a mixture of **1**•[D][C_5F_4N] and **1**•[H][$C_6F_4CF_3$] formed only D–C_5F_4N (**3a**-*d*) and H–$C_6F_4CF_3$ (**3b**) with no evidence for crossover products H–C_5F_4N (**3a**) or D–$C_6F_4CF_3$ (**3b**-*d*) (Figure 4b). Taken together, the foregoing lines of evidence inform the conclusion that the C–H RE from **1**•[H][C_5F_4E] proceeds via a unimolecular ligand coupling event.

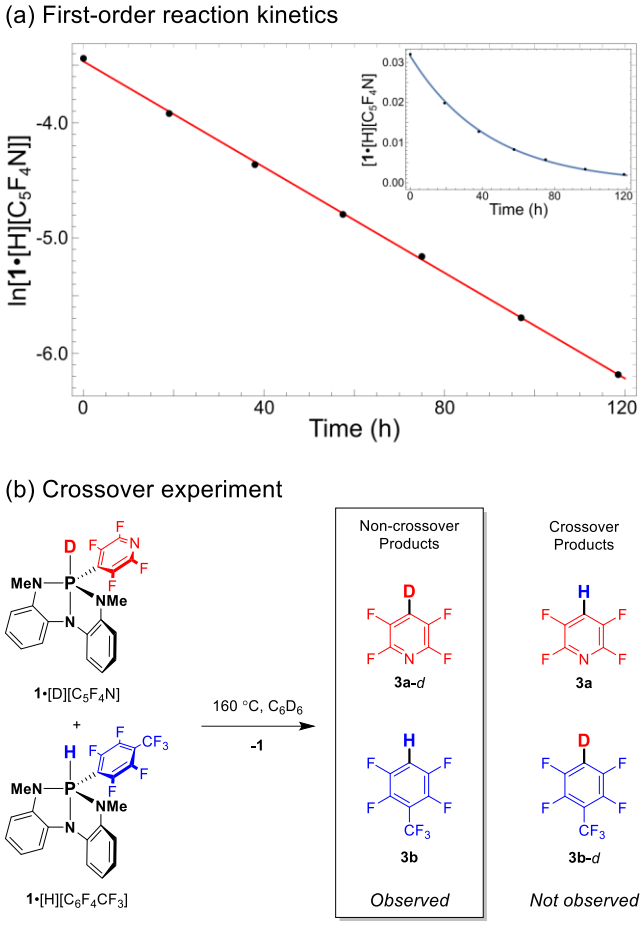

Figure 4. Experimental studies to probe into the mechanism of the H–C_5F_4E reductive elimination from **1**•[H][C_5F_4E]. (a) The first-order reaction kinetics with respect to [**1**•[H][C_5F_4N]]. (b) Crossover experiment with **1**•[D][C_5F_4N] and **1**•[H][$C_6F_4CF_3$] producing only non-crossover products.

Although a direct apical-equatorial ligand coupling is forbidden on orbital symmetry grounds,[41] DFT modelling (ωB97X-D3/def2-TZVP) identifies two candidate pathways describing concerted (albeit highly asynchronous) C–H RE mechanisms from **1**•[H][C_5F_4N]. In the first pathway, the incipient C–H bond is substantially developed prior to P–C bond cleavage in the transition structure (**TS1**, Figure 5, top). In effect, the RE has substantial character of a hydride migration from phosphorus to the carbon in the fluoroaryl group via an addition to the aromatic π^*-orbital reminiscent of concerted S_NAr[42] (see SI for details). Despite an apparent increase in $P_1–C_1$ bond order near the saddle point, no stationary point corresponding to a stable phosphonium intermediate is obtained along the reaction coordinate. Although analogous mechanisms have been suggested for other phosphorus-based ligand coupling reactions,[12,20] the high energy of this transition state ($\Delta G^{\ddagger}_{TS1}$ = 49.2 kcal/mol) likely renders such a pathway inaccessible in this case.

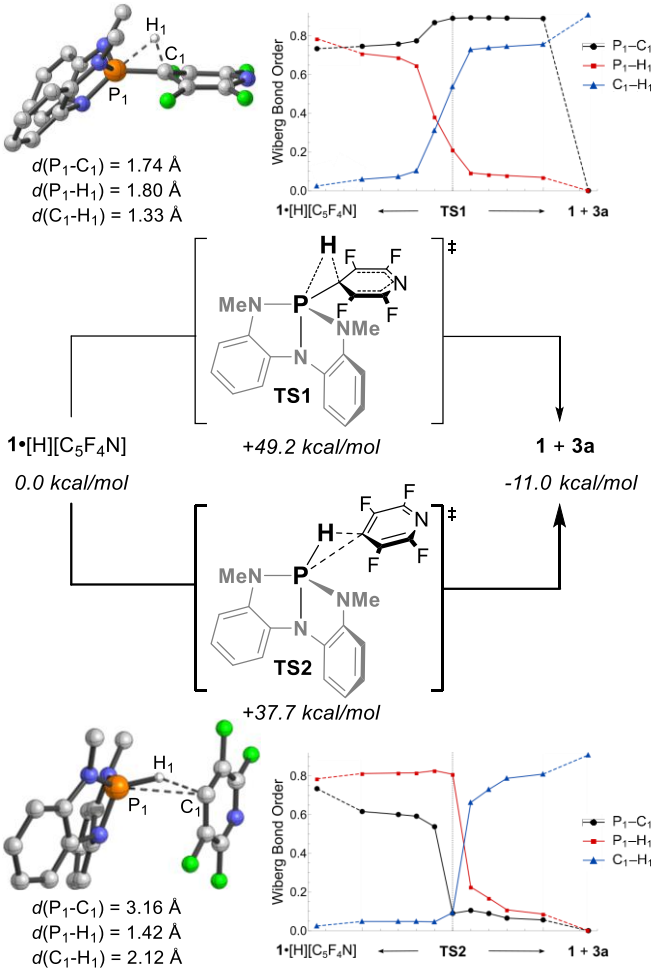

Figure 5. DFT pathways for C–H reductive elimination from **1**•[H][C_5F_4N] at the ωB97X-D3/def2-TZVP level of theory (Gibbs free energies in italics). (top) Model of **TS1** and mapping of key bond orders along the intrinsic reaction coordinates. (bottom) Model of **TS2** and mapping of key bond orders along the intrinsic reaction coordinates.

A second transition state (**TS2**, Figure 5, bottom), also located as a stationary point on the potential energy surface but lower in energy ($\Delta G^{\ddagger}_{TS2}$ = +37.7 kcal/mol), is distinguished by both the sequencing of the asynchronous bond making/breaking stages along the reaction coordinate and by the polarity of reacting P–H moiety. In **TS2**, P_1–C_1 bond elongation ($d(P_1–C_1)$ = 3.16 Å) precedes P_1–H_1 cleavage; the P_1–H_1 distance (1.42 Å) is essentially identical to starting material **1**•[H][C_5F_4N] ($d(P_1–H_1)$ = 1.42 Å). According to the natural bond orbital analysis on **TS2**, natural population analysis assigns protic character to H_1 (+0.080) and a significant second-order perturbation (17.3 kcal/mol) between the C_1 lone pair and a P_1–H_1 σ^* orbital is detected. In effect, this RE—although concerted—proceeds with high asynchronicity and resides near the boundary with a stepwise polar heterolysis/deprotonation pathway. The ensemble of experimental observations obtained to date—the temperature of reaction, kinetic unimolecularity, lack of crossover—are most consistent with **TS2** representing the operative pathway for this C–H RE.[43]

In sum, the foregoing results thus transit a closed P^{III}/P^{V} synthetic cycle for hydrodefluorination via C–F oxidative addition, F→H ligand metathesis, and C–H reductive elimination at a nontrigonal phosphorus triamide **1**. The sequencing of these elementary reactions at phosphorus is reminiscent of the role played by transition metals in aryl C–X substitution reactions,[44] but is without precedent for *p*-block compounds. The closed synthetic loop—beginning and ending with **1**—suggests that iterative cycling (i.e. catalysis) is in principle possible, but unfortunately the thermal instability of DIBAL-H is not compatible with the elevated temperature needed to promote C–H reductive elimination in this system. That said, our mechanistic models for concerted asynchronous C–H reductive elimination provide a basis for evaluating the impact of tailored alterations to **1** on the kinetics of reductive elimination with the purpose of enabling swifter C–H and related reductive elimination processes in a catalytic fashion.

ASSOCIATED CONTENT

Supporting Information

The Supporting Information is available free of charge on the ACS Publications website.

Experimental procedures; crystallographic details; computational details; IR spectra; ^{1}H, ^{13}C, ^{19}F, and ^{31}P NMR spectra (PDF)

Crystallographic data for $C_{19}H_{14}F_5N_4P$ (CIF)

Crystallographic data for $C_{19}H_{15}F_4N_4P$ (CIF)

Crystallographic data for $C_{21}H_{14}F_8N_3P$ (CIF)

Crystallographic data for $C_{21}H_{14}F_5N_4P$ (CIF)

AUTHOR INFORMATION

Corresponding Author

*radosevich@mit.edu

Notes

The authors declare no competing financial interests.

ACKNOWLEDGMENT

Financial support was provided by NSF (CHE-1900060). S.L. acknowledges the ILJU Academy and Culture Foundation for academic year fellowship support and Masamune Memorial Fellowship for summer fellowship support. S.L. appreciates Soonhyoung Kwon (MIT Chemical Engineering) for assistance in experimental setup for reaction kinetics. We are grateful to Dr. Peter Mueller, Dr. Seung Jun Hwang, Gregory T. Cleveland, and Akira Tanushi for assistance in collecting and processing crystal structure data. ChemMatCARS Sector 15 is principally supported by the Divisions of Chemistry (CHE) and Materials Research (DMR), National Science Foundation, under grant number NSF/CHE1346572. Use of the PILATUS3 X CdTe 1M detector is supported by the National Science Foundation under the grant number NSF/DMR-1531283. Use of the Advanced Photon Source, an Office of Science User Facility operated for the U.S. Department of Energy (DOE) Office of Science by Argonne National Laboratory, was supported by the U.S. DOE under Contract No. DE-AC02-06CH11357.

REFERENCES

[1] Kohei, T.; Miyaura, N. Introduction to Cross-Coupling Reactions. In *Cross-Coupling Reactions: A Practical Guide*; Miyaura, N., Ed.; Topics in Current Chemistry; Springer: Berlin, Heidelberg, 2002; pp 1–9.

[2] Chu, T.; Nikonov, G. I. Oxidative Addition and Reductive Elimination at Main-Group Element Centers. *Chem. Rev.* **2018**, *118* (7), 3608–3680.

[3] Weetman, C.; Inoue, S. The Road Travelled: After Main-Group Elements as Transition Metals. *ChemCatChem* **2018**, *10* (19), 4213–4228.

[4] Jana, A.; Samuel, P. P.; Tavčar, G.; Roesky, H. W.; Schulzke, C. Selective Aromatic C–F and C–H Bond Activation with Silylenes of Different Coordinate Silicon. *J. Am. Chem. Soc.* **2010**, *132* (29), 10164–10170.

[5] Samuel, P. P.; Singh, A. P.; Sarish, S. P.; Matussek, J.; Objartel, I.; Roesky, H. W.; Stalke, D. Oxidative Addition Versus Substitution Reactions of Group 14 Dialkylamino Metalylenes with Pentafluoropyridine. *Inorg. Chem.* **2013**, *52* (3), 1544–1549.

[6] R. Crimmin, M.; J. Butler, M.; P. White, A. J. Oxidative Addition of Carbon–Fluorine and Carbon–Oxygen Bonds to Al(I). *Chem. Commun.* **2015**, *51* (88), 15994–15996.

[7] Chu, T.; Boyko, Y.; Korobkov, I.; Nikonov, G. I. Transition Metal-like Oxidative Addition of C–F and C–O Bonds to an Aluminum(I) Center. *Organometallics* **2015**, *34* (22), 5363–5365.

[8] Styra, S.; Melaimi, M.; Moore, C. E.; Rheingold, A. L.; Augenstein, T.; Breher, F.; Bertrand, G. Crystalline Cyclic (Alkyl)(Amino)Carbene-Tetrafluoropyridyl Radical. *Chem. – Eur. J.* **2015**, *21* (23), 8441–8446.

[9] N. Swamy, V. S. V. S.; Parvin, N.; Raj, K. V.; Vanka, K.; Sen, S. S. C(sp^3)–F, C(sp^2)–F and C(sp^3)–H Bond Activation at Silicon(II) Centers. *Chem. Commun.* **2017**, *53* (71), 9850–9853.

[10] Ganesamoorthy, C.; Loerke, S.; Gemel, C.; Jerabek, P.; Winter, M.; Frenking, G.; Fischer, R. A. Reductive Elimination: A Pathway to Low-Valent Aluminium Species. *Chem. Commun.* **2013**, *49* (28), 2858–2860. (b) Urwin, S. J.; Rogers, D. M.; Nichol, G. S.; Cowley, M. J. Ligand Coordination Modulates Reductive Elimination from Aluminium(III). *Dalton Trans.* **2016**, *45* (35), 13695–13699.

[11] Tolentino, D. R.; Neale, S. E.; Isaac, C. J.; Macgregor, S. A.; Whittlesey, M. K.; Jazzar, R.; Bertrand, G. Reductive Elimination at Carbon under Steric Control. *J. Am. Chem. Soc.* **2019**, *141* (25), 9823–9826.

[12] Finet, J.-P. Ligand Coupling Reactions with Heteroatomic Compounds; Pergamon, 1998.

[13] Oae, S. Ligand Coupling Reactions Through Hypervalent and Similar Valence-Shell Expanded Intermediates. *Croat. Chem. Acta* **1986**, *59* (1), 129–151.

[14] Sagae, T.; Ogawa, S.; Furukawa, N. Stereochemical Proof for Front Side Deuteride Attack via σ-Sulfurane in the Reductive Desulfinylation of Sulfoxides with Lithium Aluminum Deuteride. *Tetrahedron Lett.* **1993**, *34* (25), 4043–4046.

[15] Crivello, J. V. Redox Initiated Cationic Polymerization: Reduction of Diaryliodonium Salts by 9-BBN. *J. Polym. Sci. Part Polym. Chem.* **2009**, *47* (21), 5639–5651.

[16] Dunn, N. L.; Ha, M.; Radosevich, A. T. Main Group Redox Catalysis: Reversible PIII/PV Redox Cycling at a Phosphorus Platform. *J. Am. Chem. Soc.* **2012**, *134* (28), 11330–11333.

[17] Reichl, K. D.; Dunn, N. L.; Fastuca, N. J.; Radosevich, A. T. Biphilic Organophosphorus Catalysis: Regioselective Reductive Transposition of Allylic Bromides via P^{III}/P^{V} Redox Cycling. *J. Am. Chem. Soc.* **2015**, *137* (16), 5292–5295.

[18] Nykaza, T. V.; Harrison, T. S.; Ghosh, A.; Putnik, R. A.; Radosevich, A. T. A Biphilic Phosphetane Catalyzes N–N Bond-Forming Cadogan Heterocyclization via P^{III}/P^{V}═O Redox Cycling. *J. Am. Chem. Soc.* **2017**, *139* (20), 6839–6842.

[19] Nykaza, T. V.; Cooper, J. C.; Li, G.; Mahieu, N.; Ramirez, A.; Luzung, M. R.; Radosevich, A. T. Intermolecular Reductive C–N Cross Coupling of Nitroarenes and Boronic Acids by P^{III}/P^{V}═O Catalysis. *J. Am. Chem. Soc.* **2018**, *140* (45), 15200–15205.

[20] Hilton, M. C.; Zhang, X.; Boyle, B. T.; Alegre-Requena, J. V.; Paton, R. S.; McNally, A. Heterobiaryl Synthesis by Contractive C–C Coupling via P(V) Intermediates. *Science* **2018**, *362* (6416), 799–804.

[21] Planas, O.; Wang, F.; Leutzsch, M.; Cornella, J. Fluorination of Arylboronic Esters Enabled by Bismuth Redox Catalysis. *Science* **2020**, *367* (6475), 313–317.

[22] McCarthy, S. M.; Lin, Y.-C.; Devarajan, D.; Chang, J. W.; Yennawar, H. P.; Rioux, R. M.; Ess, D. H.; Radosevich, A. T. Intermolecular N–H Oxidative Addition of Ammonia, Alkylamines, and Arylamines to a Planar σ^3-Phosphorus Compound via an Entropy-Controlled Electrophilic Mechanism. *J. Am. Chem. Soc.* **2014**, *136* (12), 4640–4650.

[23] Zhao, W.; McCarthy, S. M.; Lai, T. Y.; Yennawar, H. P.; Radosevich, A. T. Reversible Intermolecular E–H Oxidative Addition to a Geometrically Deformed and Structurally Dynamic Phosphorous Triamide. *J. Am. Chem. Soc.* **2014**, *136* (50), 17634–17644.

[24] Robinson, T. P.; De Rosa, D. M.; Aldridge, S.; Goicoechea, J. M. E–H Bond Activation of Ammonia and Water by a Geometrically Constrained Phosphorus(III) Compound. *Angew. Chem. Int. Ed.* **2015**, *54* (46), 13758–13763.

[25] Uchida, Y.; Onoue, K.; Tada, N.; Nagao, F.; Oae, S. Ligand Coupling Reaction on the Phosphorus Atom. *Tetrahedron Lett.* **1989**, *30* (5), 567–570.

[26] For mechanistically distinct hydrodefluorination catalyzed by *p*-block Lewis acids, see: (a) Caputo, C. B.; Hounjet, L. J.; Dobrovetsky, R.; Stephan, D. W. Lewis Acidity of Organofluorophosphonium Salts: Hydrodefluorination by a Saturated Acceptor. *Science* **2013**, *341* (6152), 1374–1377. (b) Stahl, T.; Klare, H. F. T.; Oestreich, M. Main-Group Lewis Acids for C–F Bond Activation. *ACS Catal.* **2013**, *3* (7), 1578–1587.

[27] Chen, W.; Bakewell, C.; Crimmin, M. Functionalisation of Carbon–Fluorine Bonds with Main Group Reagents. *Synthesis* **2016**, *49* (04), 810–821.

[28] Competition experiments among the perfluoroarene substrates investigated at 70 °C revealed the following qualitative ordering of reactivity: perfluorobenzonitrile > pentafluoropyridine > octafluorotoluene.

[29] Selective C–F OA at the 4-position was also observed in reactions with 2,4,6-trifluoropyridine (^{31}P δ -56.3 ppm, $^1J_{P-F}$ = 798 Hz) and 3,4,5-trifluoropyridine (^{31}P δ -60.0 ppm, $^1J_{P-F}$ = 769 Hz) in tetrahydrofuran at 150 °C, although accompanied by unidentified side reactions.

[30] (a) Arévalo, A.; Tlahuext-Aca, A.; Flores-Alamo, M.; García, J. J. On the Catalytic Hydrodefluorination of Fluoroaromatics Using Nickel Complexes: The True Role of the Phosphine. *J. Am. Chem. Soc.* **2014**, *136* (12), 4634–4639. (b) Facundo, A. A.; Arévalo, A.; Fundora-Galano, G.; Flores-Álamo, M.; Orgaz, E.; García, J. J. Hydrodefluorination of Functionalized Fluoroaromatics with Triethylphosphine: A Theoretical and Experimental Study. *New J. Chem.* **2019**, *43* (18), 6897–6908.

[31] For examples of OA of non-aryl C–F bonds to σ^3-P compounds, see: (a) Weiss, J.-V.; Schmutzler, R. Formation of a Carbon–Phosphorus Bond between a C–F Compound and Phosphorus(III) Fluorides: A Fluorine Analogue of the Kinnear–Perren Reaction Furnishing 1-Adamantylfluorophosphoranes. *J. Chem. Soc. Chem. Commun.* **1976**, *0* (16), 643–644. (b) Burton, D. J.; Shinya, S.; Howells, R. D. The Role of α and β Fluorine in Product Determination of Fluoro Olefin-Tertiary Phosphine Reactions. Ylide vs. Vinylphosphorane Formation. *J. Am. Chem. Soc.* **1979**, *101* (13), 3689–3690. (c) Plack, V.; Goerlich, J. R.; Thönnessen, H.; Jones, P. G.; Schmutzler, R. Air-Stable Trifluorophosphoranes: Preparation, X-Ray Crystal Structure Determinations, and Reactions. *Z. Für Anorg. Allg. Chem.* **1999**, *625* (8), 1278–1286. (d) Keßler, M.; Neumann, B.; Stammler, H.-G.; Hoge, B. Fluorotrimethyl[(Z)-Pentafluoropropen-1-Yl]Phosphorane: Structure, Bonding, and Reactivity. *Z. Für Anorg. Allg. Chem.* **2020**, *646*, 1–7.

[32] Lee, K.; Blake, A. V.; Tanushi, A.; McCarthy, S. M.; Kim, D.; Loria, S. M.; Donahue, C. M.; Spielvogel, K. D.; Keith, J. M.; Daly, S. R.; Radosevich, A. T. Validating the Biphilic Hypothesis of Nontrigonal Phosphorus(III) Compounds. *Angew. Chem. Int. Ed.* **2019**, *58* (21), 6993–6998.

[33] $P(NMePh)_3$ was unreactive under the same reaction conditions. For the reaction of $P(NEt_2)_3$ with **2a**, see: Gutov, A. V.; Rusanov, E. B.; Ryabitskii, A. B.; Chernega, A. N. Octafluoro-4,4′-Bipyridine and Its Derivatives: Synthesis, Molecular and Crystal Structure. *J. Fluor. Chem.* **2010**, *131* (2), 278–281.

[34] $\tau = (\angle N_1–P_1–F_1/H_1 - \angle N_2–P_1–F_3)/60°$. For the definition of τ, see: Addison, A. W.; Rao, T. N.; Reedijk, J.; Rijn, J. van; Verschoor, G. C. Synthesis, Structure, and Spectroscopic Properties of Copper(II) Compounds Containing Nitrogen–Sulphur Donor Ligands; the Crystal and

Molecular Structure of Aqua[1,7-Bis(N-Methylbenzimidazol-2′-Yl)-2,6-Dithiaheptane]Copper(II) Perchlorate. *J. Chem. Soc. Dalton Trans.* **1984**, No. 7, 1349–1356.

[35] Groom, C. R.; Bruno, I. J.; Lightfoot, M. P.; Ward, S. C. The Cambridge Structural Database. *Acta Crystallogr. Sect. B Struct. Sci. Cryst. Eng. Mater.* **2016**, *72* (2), 171–179.

[36] Kornath, A.; Neumann, F.; Oberhammer, H. Tetramethylphosphonium Fluoride: "Naked" Fluoride and Phosphorane. *Inorg. Chem.* **2003**, *42* (9), 2894–2901. The P–F_{ax} IR stretching frequencies are taken as the average of symmetric and asymmetric vibrational modes.

[37] Howell, J. M. Bond Length Variations in Substituted Phosphoranes. *J. Am. Chem. Soc.* **1975**, *97* (14), 3930–3933.

[38] Cleveland, G. T.; Radosevich, A. T. A Nontrigonal Tricoordinate Phosphorus Ligand Exhibiting Reversible "Nonspectator" L/X-Switching. *Angew. Chem. Int. Ed.* **2019**, *58* (42), 15005–15009.

[39] Erdmann, P.; Leitner, J.; Schwarz, J.; Greb, L. An Extensive Set of Accurate Fluoride Ion Affinities for P-Block Element Lewis Acids and Basic Design Principles for Strong Fluoride Ion Acceptors. *ChemPhysChem* **2020**, *21* (10), 987–994.

[40] For a review discussing KIEs in C–H reductive elimination, see: Gómez-Gallego, M.; Sierra, M. A. Kinetic Isotope Effects in the Study of Organometallic Reaction Mechanisms. *Chem. Rev.* **2011**, *111* (8), 4857–4963.

[41] Hoffmann, R.; Howell, J. M.; Muetterties, E. L. Molecular Orbital Theory of Pentacoordinate Phosphorus. *J. Am. Chem. Soc.* **1972**, *94* (9), 3047–3058.

[42] (a) Kwan, E. E.; Zeng, Y.; Besser, H. A.; Jacobsen, E. N. Concerted Nucleophilic Aromatic Substitutions. *Nat. Chem.* **2018**, *10* (9), 917–923. (b) Rohrbach, S.; Smith, A. J.; Pang, J. H.; Poole, D. L.; Tuttle, T.; Chiba, S.; Murphy, J. A. Concerted Nucleophilic Aromatic Substitution Reactions. *Angew. Chem. Int. Ed.* **2019**, *58* (46), 16368–16388.

[43] H/D kinetic isotope effect (KIE) values were computed from DFT for both **TS1** (1.18) and **TS2** (1.02); see SI for details. The similarity of these values, which both conform qualitatively with the experimental KIE, prohibit a decisive differentiation between these mechanisms based on this metric.

[44] Ahrens, T.; Kohlmann, J.; Ahrens, M.; Braun, T. Functionalization of Fluorinated Molecules by Transition-Metal-Mediated C–F Bond Activation To Access Fluorinated Building Blocks. *Chem. Rev.* **2015**, *115* (2), 931–972.

TOC Graphic